The Impact of Increasing Stratospheric Radiative Damping on the QBO Period

Tiehan Zhou[1,2], Kevin DallaSanta[1,3], Larissa Nazarenko[1,2], Gavin A. Schmidt[1], Zhonghai Jin[1]

[1]NASA Goddard Institute for Space Studies, New York, NY
[2]Center for Climate Systems Research, Columbia University, New York, NY
[3]Universities Space Research Association, Columbia, MD

Correspondence to: Tiehan Zhou (tz2131@columbia.edu)

Abstract. Stratospheric radiative damping increases as atmospheric carbon dioxide concentration rises. We use the one-dimensional mechanistic models of the QBO to conduct sensitivity experiments and find that the simulated QBO period shortens due to the enhancing of radiative damping in the stratosphere. This result suggests that increasing stratospheric radiative damping due to rising CO_2 may play a role in determining the QBO period in a warming climate along with wave momentum flux entering the stratosphere and tropical vertical residual velocity, both of which also respond to increasing CO_2.

1. Introduction

The quasi-biennial oscillation (QBO) dominates the variability of the equatorial middle and lower stratosphere and is characterized by a downward propagating zonal wind regime that regularly changes from westerlies to easterlies. The QBO period ranges from 22 to 34 months with its average being slightly longer than 28 months. The QBO not only manifests itself in the equatorial zonal winds, but also leaves an imprint on the temperature in both the tropics and extratropics (Baldwin et al., 2001 and references therein).

The QBO has far-reaching implications for global weather and climate systems. First of all, the QBO exerts a marked influence on the distribution and transport of various chemical constituents such as ozone (O_3) (e.g., Hasebe, 1994), water vapor (H_2O) (e.g., Kawatani et al., 2014), methane (CH_4), nitrous oxide (N_2O), hydrogen fluoride (HF), hydrochloric acid (HC1), odd nitrogen species (NO_y) (e.g., Zawodny and McCormick, 1991), and volcanic aerosol (Trepte and Hitchman, 1992). Secondly, it is well appreciated that the QBO influences the extratropical circulation in the winter stratosphere, which is commonly known as the Holton–Tan effect (Holton and Tan, 1980; Labitzke, 1982). It has been noted that the effect of the QBO on the extratropical winter stratosphere impacts the severity of stratospheric ozone depletion (e.g., Lait et al., 1989). Furthermore, taking account of the QBO improves the simulation and predictability of the extratropical troposphere (e.g., Marshall and Scaife, 2009). Finally, through its modulation of temperature and vertical wind shear in the vicinity of the tropical tropopause, the QBO influences tropical moist convection (Collimore et al., 2003; Liess and Geller, 2012), the El Niño-Southern Oscillation (ENSO) (Gray et al., 1992; Huang et al., 2012; Hansen et al. 2016), the Hadley circulation (Hitchman and Huesmann, 2009), the tropospheric subtropical jet (Garfinkel and Hartmann, 2011a, 2011b), the boreal summer monsoon (Giorgetta et al., 1999), and the Madden-Julian Oscillation (Yoo and Son, 2016**)**. Intriguingly, the QBO is also reported to influence the activities of tropical cyclones (Gray et al., 1984; Ho et al., 2009), albeit this issue is still unsettled (Camargo and Sobel, 2010) and needs further study.

Efforts to understand and simulate the QBO have been ongoing ever since its discovery by Ebdon (1960) and Reed et al. (1961). Lindzen and Holton (1968) and Holton and Lindzen (1972) developed the classical theory of the QBO. Namely, as waves propagate upward, they are attenuated by thermal damping, encounter critical levels, and accelerate and decelerate the mean flow, providing momentum sources for both the westerly and easterly phases of the QBO.

Holton and Lindzen's (1972) model (hereafter referred to as HL model) was further simplified by Plumb (1977), the elegance of which made it a standard paradigm for the QBO. In Plumb's (1977) Boussinesq formulation, the QBO period is inversely dependent upon both the momentum flux and thermal dissipation rate. Hamilton (1981) further highlighted the role of the radiative damping rate on both the realistic vertical structure and the realistic period of the QBO.

By adopting higher vertical resolutions and incorporating various gravity wave parameterization schemes, many state-of-the-art climate models have shown the capability to self-consistently simulate the QBO (Scaife et al., 2000; Giorgetta et al., 2002, 2006; Rind et al., 2014, 2020; Geller et al., 2016a; Richter et al., 2020a, 2020b). Given the important implications of the QBO for the global climate system, it is natural to ask how the QBO will change in a warming climate.

Giorgetta and Doege (2005) showed a shortening of the QBO period in their doubled CO_2 experiments. They reasoned that both the weakening of the tropical upwelling and the prescribed increase of gravity wave sources lead to the reduction of the QBO period in a warming climate. However, most climate models project a strengthening rather than weakening of tropical upwelling in a warmer climate (Butchart et al., 2006; Butchart 2014; Li et al., 2008). Employing a model without any parametrized non-orographic gravity waves, Kawatani et al. (2011) demonstrated that the intensifying tropical upwelling in a warming climate dominates the counteracting effect of enhanced wave fluxes and consequently projected a lengthening of the QBO period. Using fixed sources of parametrized gravity waves, Watanabe and Kawatani (2012) also projected an elongation of the QBO period in a warming climate and ascribed it to the stronger tropical upwelling. Analyzing four Coupled Model Intercomparison Project phase 5 (CMIP5) models that could simulate a reasonable QBO, Kawatani and Hamilton (2013) found that the projected trends of the QBO period were inconsistent in sign. They further investigated the 60-year operational balloon-borne radiosonde observations provided by the Free

Berlin University and detected no significant trend in the QBO period. Richter et al. (2020b) investigated the response of the QBO to doubled and quadrupled CO_2 climates among eleven models that participated in Phase 1 of the Stratospheric-tropospheric Processes And their Role in Climate QBO-initiative (QBOi; Butchart et al., 2018), and found no consensus on how the QBO period would respond to a changing climate. Recently, Butchart et al. (2020) evaluated ten Coupled Model Intercomparison Project phase 6 (CMIP6) models with realistic QBO in two Shared Socioeconomic Pathways (SSPs, Gidden et al., 2019) scenario simulations and surprisingly found that the QBO period shortens in seven of those ten models in both in both SSP3-7.0 and SSP5-8.5 scenarios although only two and three models show a significant shortening trend in the respective scenarios.

It is challenging to ascertain the trend of the QBO period in a warming climate. On one hand, a speeding-up of the Brewer-Dobson circulation in a warming climate leads to a lengthening of the QBO period in most climate models. On the other hand, there is a robust increase in the vertical component of the EP flux for both eastward and westward propagating waves (Richter et al., 2020b; Butchart et al., 2020), indicating that the QBO period shortens due to the enhanced wave driving in a warming climate. The competing effects between enhanced wave driving and a faster Brewer-Dobson circulation suggests that trends in the QBO period are likely to be small and difficult to detect due to the large cycle-to-cycle variability that is reproduced by climate models (Butchart et al., 2020). In addition, uncertainty in the representation of the parameterized gravity waves make it more elusive to detect the trend of the QBO period in a warming climate (Schirber et al., 2015; Richter et al., 2020b).

Given the fact that the QBO period is influenced by the radiative damping (Plumb 1977; Hamilton 1981), a natural question to ask is whether it could play a role on the trend of the QBO in a warming climate. Fels (1985) estimated that the radiative damping time under a doubling of CO_2 would decrease

by about 23%. His estimate implies a shortening of the QBO period as the radiative damping rate increases.

It is well-known that enhanced wave fluxes entering the stratosphere and stronger tropical upwelling individually play a dominant role in determining the trends in the QBO period in a warming climate. Does the competing effect between them leave some room for increasing stratospheric radiative damping to exert an influence on the QBO period? In this paper, we use the HL model to isolate the effect of radiative damping on the QBO period by assuming that the momentum flux entering the stratosphere doesn't change in our experiments. Observational and modeling studies (Andrews et al., 1987; Kawatani et al., 2009, 2010, 2011; Richter et al., 2020b; Holt et al., 2020) showed that the wave forcing spectrum is similar to a discrete two-wave spectrum rather than red-noise or white-noise, all of which are illustrated in Saravanan (1990). Accordingly, the QBO is indeed sensitive to stratospheric radiative damping, and the HL model is suitable for us to conduct the sensitivity analysis.

The remainder of this paper is organized as follows. Section 2 investigates the sensitivity of the QBO period to the radiative damping using HL's original model. Section 3 explores the sensitivity of the QBO period to the radiative damping using a modified HL model where the semiannual forcing is removed. Discussion and conclusions are presented in Sections 4 and 5 respectively.

2. Sensitivity of the QBO period to enhanced stratospheric radiative damping in the original HL model

In the HL model the governing equation of mean flow emerges after the primitive momentum equation is meridionally averaged over some suitable latitudinal belt over the equator.

$$\frac{\partial \overline{u}}{\partial t} = -\frac{1}{\rho_0}\frac{\partial}{\partial z}\left[\sum_{i=0}^{1}\overline{F_i}\right] + K_z\frac{\partial^2 \overline{u}}{\partial z^2} + G \qquad (1)$$

where $\overline{u}$ is mean zonal wind, ρ_0 is mean density, $\overline{F_i}$ is the meridionally averaged vertical Eliassen-Palm flux associated with wave i, the index i refers to the individual waves, K_z is a vertical eddy diffusion coefficient, t is time, z is altitude, and G is semiannual forcing identical to that specified by HL.

The $\overline{F_i}$ is are evaluated with Lindzen's (1971) WKB formalism for equatorial waves in shear. When only infrared cooling acts to damp the waves the formulae for $\overline{F_i}$ are

$$\overline{F_0}(z) = A_0\, exp\left(- \int_{17km}^{z} \frac{\alpha N}{k(c-\overline{u})^2}\, dz \right) \tag{2}$$

for the Kelvin wave, and

$$\overline{F_1}(z) = A_1\, exp\left[- \int_{17km}^{z} \frac{\alpha\beta N}{k^3(c-\overline{u})^3}\left(1 - \frac{k^2(\overline{u}-c)}{\beta}\right) dz \right] \tag{3}$$

for the mixed Rossby-gravity wave. As in HL, the wavenumber k, the phase speed c, and A_0 are chosen to be $2\pi/(40{,}000\text{ km})$, 30 m s^{-1}, and 0.04 m^2 s$^{-2}\rho_0(17\text{ km})$, respectively for the Kelvin wave while they are equal to $-2\pi/(10{,}000\text{ km})$, -30 m s^{-1}, and -0.04 m^2 s$^{-2}\rho_0(17\text{ km})$, respectively for the mixed Rossby-gravity wave. In Eq. (1), $K_z = 0.3$ m^2 s^{-1}, which is also the same as in HL. In addition, $\beta = 2\Omega/a$, where Ω is earth's rotation rate, and a is earth's radius. HL's boundary conditions stipulated that $\overline{u} = 0$ at the lowest model level (17 km) and constrained $\overline{u}$ to vary semiannually at the top level (35 km).

In our control run that is used to depict the present-day QBO all the model parameters are identical to those used by HL in their original simulation. The Brunt-Väisälä frequency

$$N = \sqrt{\frac{g}{T_0}\left(\frac{dT_0}{dz} + \frac{g}{c_p}\right)} \tag{4}$$

In Eq. (4), g is gravity, T_0 is mean temperature, and c_p is specific heat of dry air at constant pressure. HL set N in Eq. (4) to $2.16 \times 10^{-2}\text{s}^{-1}$ with a scale height $H = 6$ km. In addition, the Newtonian

cooling profile in our control run, i.e., $\alpha(z)$ in Eqs. (2) and (3), is also identical to that in the original HL model and depicted in FIG. 1a as the black line. Namely, $\alpha(z)$ in the control run increases from $(21\ \text{day})^{-1}$ at 17 km to $(7\ \text{day})^{-1}$ at 30 km and is kept at $(7\ \text{day})^{-1}$ between 30 km and 35 km. Fels (1985) explained why the magnitude of this radiative damping rate is suitable for simulating the QBO on the basis of the scale-dependent effect of radiative damping (Fels, 1982). Hamilton (1981) demonstrated that the proper choice of $\alpha(z)$ is crucial in simulating a realistic vertical structure of the QBO.

Eq. (1) was integrated for 100 years using the forward-backward scheme (Matsuno, 1966). The vertical resolution was 250 m and identical to that in HL. The time step was 12 hr, i.e., one half of used in HL, because the 24-hr time step resulted in numerical instability in our integration.

FIG. 2a shows the time–height section of the monthly averaged mean zonal wind simulated over the first 20 years using the HL model. Both the QBO and the semiannual oscillation (SAO) are conspicuous. The fast Fourier transform (FFT) method is used to calculate the frequency power spectra. In order to more accurately derive the QBO period, the model was run for 100 years to increase the spectral resolution. Frequency–height sections of the power spectral densities (PSD) over zero to the Nyquist frequency, i.e., 0.5 cycle/month, depict two sharp lines (peaks) at $\frac{1}{30}$ and $\frac{1}{6}$ cycle/month, respectively (not shown). In order to better visualize the magnitudes of the PSD, we show two truncated frequency–height sections with FIG. 2b and FIG. 2c highlighting the QBO and the SAO respectively. FIG. 2b shows that the QBO dominates over the model domain. The peak frequency corresponds to the period of 30 months. FIG. 2c shows the SAO dominates near the model top due to the fact a semiannual forcing was imposed in the altitudes from 28 to 35 km.

It is worth mentioning that the QBO period shown here is longer than 26.5 months reported in the HL paper (see their FIG. 1). Using the HL model parameters, the QBO period simulated by Plumb (1977)

was close to three years (refer to his FIG. 8a), which is longer than our simulated QBO period, i.e., 30.0 months. Although we could not explain why our simulated QBO period is longer than that simulated by HL, we found that when the upper boundary condition is changed from $\overline{u} = 14 \sin(\omega_a t)$ and $\omega_a = \frac{2\pi}{180}$ day^{-1} used in the HL's original model (refer to their Eqs. (2)) to $\frac{\partial \overline{u}}{\partial z} = 0$ used in Plumb (1977), the simulated QBO period becomes 34.3 month (figure not shown). In other words, when we adopted the stress-free upper boundary condition as in Plumb (1977), our simulated QBO period is comparable to that simulated by him, which lends credence to our reconstruction of the HL model.

In order to rigorously quantify the relationship of the Newtonian cooling coefficient at any altitude z between the reference and doubled CO_2, we follow Dickinson (1973) in using a radiative transfer model to calculate $Q_1(T)$ for a reference temperature profile $T(z)$ and $Q_1(T+\delta)$ for $T(z)+\delta$, where a small perturbation $\delta T = 0.1\ K$ with $T(z)$ being the 1976 U.S. standard atmosphere. Our radiative transfer computations use the MODTRAN gas absorption database with 0.1 cm^{-1} spectral resolution (Jin et al. 2019; Berk et al. 2008). We then repeat the computations with the doubled CO_2 to yield $Q_2(T)$ and $Q_2(T+\delta)$. It follows that $\frac{\alpha_2}{\alpha_1} = \frac{Q_2(T+\delta) - Q_2(T)}{Q_1(T+\delta) - Q_1(T)}$, where $\alpha_1(z)$ and $\alpha_2(z)$ stand for the Newtonian cooling coefficient at any altitude z for the reference and doubled CO2, respectively. In FIG. 1b the black line depicts the ratio for the broadband longwave radiation ($5\ \mu m - 100\ \mu m$) and the red line delineates the ratio for the CO_2 absorption band ($12\ \mu m - 18\ \mu m$). The ratio calculated over the broadband is conspicuously smaller than that for the CO_2 absorption band, because the changes in cooling rate from the temperature perturbation are larger over a wider spectral band. It is worth mentioning that the ratios calculated over the broadband in the middle stratosphere are close to 1.3 and comparable to what Fels (1985) estimated, i.e., about 23% decrease of the radiative damping time under a doubling of CO_2.

Returning to the 1D HL model, we synthesize those findings by prescribing $\alpha_2(z)$ in our experimental runs for the doubled CO_2 as follows: an increase of 30% between 30 and 35 km, no change

219 below 24 km, and linear interpolation between 24 and 30 km. The resulting increase of radiative damping
220 rate from the control runs is depicted as the red line in FIG. 1a. This increase is reasonable based on our
221 results shown in FIG. 1b.

222 FIG. 3a shows the time–height section of the monthly averaged mean zonal wind simulated over the
223 first 20 years for the doubled CO_2 run, where the increased $\alpha(z)$ depicted as the red line in FIG. 1a was
224 employed while all other parameters are identical to those in the control run. Obviously, the QBO
225 dominates below 28 km while the semiannual oscillation (SAO) dominates above 31 km. Like FIG. 2b
226 and FIG. 2c, we only show two truncated frequency–height sections with FIG. 3b highlighting the QBO
227 and FIG. 3c highlighting the SAO. FIG. 3b also shows that the QBO prevails over the model domain. The
228 peak frequency corresponds to the period of 27.9 months. FIG. 3c shows the SAO dominates near the
229 model top due to the same imposed semiannual forcing as that in the control run.

230 In summary, using the original HL model we found that the increased radiative damping due to the
231 doubling of CO2 shortens the QBO period by 7% (i.e., decreases from 30 months to 27.9 months).

232

233 **3. Sensitivity of the QBO period to enhanced stratospheric radiative damping in the modified HL**
234 **model without the semiannual forcing**

235 HL pointed out that the imposed semiannual oscillation was not essential for their QBO theory.
236 Applying $\frac{\partial \overline{u}}{\partial z} = 0$ as the upper boundary condition, Plumb (1977) showed a simulated QBO without
237 resorting to the semiannual momentum source (refer to his FIG. 8b). In the following control run, all
238 parameters are identical to those used in the previous control run in Section 2 except that G in Eq. (1) is
239 set to zero with $\frac{\partial \overline{u}}{\partial z}$ also being set to zero at $z = 35$ km. Hereafter we refer to it as the Plumb model[1]. FIG.

[1] Strictly speaking, it is the HL model modified by Plumb (1977). In this paper, we don't use his eponymous model, i.e., the simplest possible model of the QBO, where Boussinesq fluids with uniform mean density were employed, because the HL model and its variant are considerably more realistic.

4a shows the time–height section of the monthly averaged mean zonal wind simulated over the first 20 years using the Plumb model. As expected, the QBO emerges without any trace of SAO since $G = 0$ in Eq. (1). FIG. 4b shows that the QBO dominates over the whole model domain. The peak frequency corresponds to the period of 37.5 months, which is comparable to that simulated by Plumb (1977) shown in his FIG. 8b. Apparently, the QBO period from the Plumb model, i.e., 37.5 months shown in FIG. 4b, is longer than that from the HL model, i.e., 30.0 months shown in FIG. 2b. This is partly because the additional forcing G in Eq. (1) was removed in the Plumb model.

In the following experimental run, all parameters are identical to those used in the previous experimental run in Section 2 except that G in Eq. (1) is set to zero with $\frac{\partial \overline{u}}{\partial z}$ also being set to zero at $z = 35\ \mathrm{km}$. In other words, the following experimental run using the Plumb model employed the same parameters as the afore-mentioned control run using the Plumb model except that the increased $\alpha(z)$ shown as the red line in FIG. 1a was used in the following experimental run while $\alpha(z)$ shown as the black line in FIG. 1a was used in the above control run. FIG. 5a shows the time–height section of the monthly averaged mean zonal wind simulated over the first 20 years for the doubled CO_2 run. It is natural that only the QBO emerges. A comparison of FIG. 4a and FIG. 5a shows that the QBO period shortens when the infrared damping increases in response to the doubled CO2. FIG. 5b shows that the QBO dominates over the whole model domain. The peak frequency corresponds to the period of 31.6 months.

Using the Plumb model, we found that the increased radiative damping due to the doubling of CO_2 shortens the QBO period by 15.7% (i.e., decreases from 37.5 months to 31.6 months).

4. Discussion

Dunkerton (1997) showed that in the presence of tropical upwelling it was gravity waves rather than large-scale Kelvin and mixed Rossby-gravity waves that contributed the bulk of QBO forcing.

263 Consequently, Geller et al. (2016a, 2016b) pointed out that enough gravity wave momentum flux is
264 required to model the QBO in a self-consistent manner in climate models and that the magnitude of the
265 subgrid-scale gravity wave momentum flux plays a crucial role in determining the QBO period. Since
266 there is no tropical upwelling in either the HL model or the Plumb model, it is natural that planetary-
267 scale Kelvin and mixed Rossby-gravity waves largely determine the QBO periods shown in Sections 2
268 and 3 due to the fact that the specified G is significantly weaker than that in the terrestrial stratosphere.
269 We conducted another sensitivity test where all parameters are identical to those in the HL model except
270 that G in both the control and experimental runs is twice as large as that used by HL. As the radiative
271 damping profile changes from the black line to the red line above 24 km shown in FIG. 1a, our simulated
272 QBO period decreases from 28.6 months to 27.3 months (figures not shown). This smaller percentage
273 decrease of 4.5% is not unexpected because G is not sensitive to the radiative damping at all and the
274 greater specified G reduces the fraction of the total wave forcing arising from the planetary waves.
275 We further conducted two sensitivity tests where all parameters are identical to those in the HL model
276 except that G in the first test is half as large as that used by HL and is equal to zero in the second test.
277 Surprisingly, as the radiative damping profile changes from the black line to the red line above 24 km
278 shown in FIG. 1a, our simulated QBO periods decreases from 30.0 months to 28.6 months both for G
279 being decreased by 50% and for $G = 0$ (figures not shown). This 4.7% decrease in the QBO period is
280 smaller than the 7% reduction obtained from the sensitivity test presented in Section 2 when G is the
281 same as that used by HL. It is surprising because the model atmosphere is expected to be more sensitive
282 to the changes in the radiative damping as G becomes smaller and smaller. Note that when our control
283 runs adopt the black radiative damping profile shown in FIG. 1a the simulated QBO periods are not
284 sensitive to the imposed semiannual forcing provided that G does not exceed the values employed by
285 HL. Similarly, when our experimental runs adopt the red radiative damping profile above 24 km shown

in FIG. 1a the simulated QBO periods are also not sensitive to the imposed semiannual forcing provided that G does not exceed 50% of the values adopted in HL. The question naturally arises: what is responsible for this unexpected behavior?

In Section 2, the simulated QBO periods are equal to 30 and 34.3 months when we adopted the no-slip and stress-free upper boundary condition respectively with all other parameters being identical to those used by HL. The results implicate the upper boundary conditions in the inconsistency. Plumb (1977) pointed out that the upper boundary in HL was undesirably low and implied that raising the lid to an additional 50% would be adequate for the robustness in his model. Here, we carry out a series of sensitivity tests by raising the model lid gradually from 35 km to 55 km with the one-kilometer increment. we will demonstrate how the behavior of the HL model with $G = 0$ converges with that of the Plumb model. The modified HL model, i.e., the HL model with $G = 0$ is identical to the Plumb model except that the former has the no-slip upper boundary condition while the latter has the stress-free upper boundary condition. Both models share the same governing equation (5). Note that we set the radiative damping rate above the 35 km level to its value at the 35 km level shown in FIG. 1a.

For the radiative damping profile corresponding to the reference CO_2, FIG. 6 shows that when the model lid is placed at the 35 km level the simulated QBO period of 30.0 months with the no-slip upper boundary condition (solid black line) is apparently shorter than that of 37.5 months with the stress-free upper boundary condition (dashed black line). FIG. 6 also shows that as the model lid is raised incrementally from the 35 km level to the 46 km level, the discrepancies between the simulated QBO periods due to the different upper boundary conditions decrease monotonically. No matter whether we adopt the no-slip or stress-free upper boundary condition, the simulated QBO period is 32.4 months for the reference radiative damping profile provided that the model top is at or above the 46 km level.

Similarly, for the radiative damping profile corresponding to the doubled CO_2, FIG. 6 demonstrates that when the model lid is placed at the 35 km level the simulated QBO period of 28.6 months with the no-slip upper boundary condition (solid red line) is obviously shorter than that of 31.6 months with the stress-free upper boundary condition (dashed red line). FIG. 6 also exhibits that as the model lid is raised gradually from the 35 km level to the 40 km level, the discrepancies between the simulated QBO periods due to the different upper boundary conditions decrease monotonically. No matter whether we adopt the no-slip or stress-free upper boundary condition, the simulated QBO period for the enhanced infrared cooling due to the doubled CO_2 is 30.0 months provided that the model top is at or above the 40 km level. It is apparent that the required model top is lower when the radiative damping is augmented due to the doubling of CO_2 because the planetary waves dissipate more steeply with height in presence of the enhanced infrared cooling rates.

FIG. 6 suggests that when the model lid is sufficiently high the QBO period in response to the enhanced radiative damping due to the increasing CO_2 will decrease from 32.4 to 30.0 months. This 7.4% decrease in the QBO period is independent of the upper boundary condition. Note that the relative uncertainty in the ratio $\frac{\alpha_2}{\alpha_1}$ calculated over the broadband (refer to the black line shown in FIG. 1b) ranges from 5% to 10% in the lower stratosphere and from 10 to 15% in the middle and upper stratosphere. Thus, the relative uncertainty in the calculated ratio is 15% at a liberal estimate in the stratosphere. Using the HL model with its top at the 48 km level, we further conducted two experiments by adopting $G = 0$ in Eq. (1) and increasing the radiative damping corresponding to the doubled CO_2 between 30 km and 48 km by $30\% - 30\% * 15\% = 25.5\%$ and $30\% + 30\% * 15\% = 34.5\%$ respectively relative to that in the control run. The simulated QBO periods are 30.3 and 29.7 months respectively. Therefore, when the model lid is sufficiently high the QBO period in response to the enhanced radiative damping due to the doubled CO_2 will decrease by approximately $7.4\% \pm 0.9\%$.

Jonsson et al. (2004) showed that the doubled CO_2 induces a substantial cooling throughout most of the middle atmosphere, which in turn increases the ozone mixing ratio by 15–20% in the upper stratosphere and by 10–15% in the lower mesosphere (refer to their Figure 6). Incorporating this increase into the ozone profile for the doubled CO_2, we recalculated the ratio of α_2, the Newtonian cooling coefficient for the doubled CO_2, to α_1, the Newtonian cooling coefficient for the reference CO_2. Our calculated α_2/α_1 is only slightly increased as compared with that shown FIG. 1b no matter whether the CO_2 absorption band is $5\ \mu m - 100\ \mu m$ or $12\ \mu m - 18\ \mu m$ (figure not shown). It is not unexpected because the infrared radiative cooling by ozone is significantly smaller than that by CO_2 (refer to Fig. 1 in Dickinson 1973) and, as a result, the 15–20% increases in the ozone mixing ratio will not make a noticeable difference. Since the monthly and zonal mean 2-D ozone concentrations are specified in about 80% of CMIP5 models (Cionni et al., 2011) and the monthly mean 3-D ozone data are employed in many CMIP6 models (Keeble et al., 2020), it is expected that the change in the radiative damping due to the increase in ozone in response to the doubled CO_2 only marginally impacts the QBO periods in those models that do not include an interactive chemistry. However, the 15–20% increases in the ozone mixing ratio in response to the doubled CO_2 do contribute the shortening of the QBO period due to its role in strengthening the tropical upwelling in the stratosphere (Bushell et al., 2010).

The real atmosphere involves the complex interactions among dynamics, chemistry, and radiation (Andrews et al., 1987). First of all, the dynamical QBO goes hand in hand with the ozone QBO (Hasebe, 1994). Shibata and Deushi (2005) pointed out that the radiative heating related to the ozone QBO could modify the secondary meridional circulation associated with the QBO, and consequently could modify how the QBO westerlies move down faster than the QBO easterlies, leading to the elongation of the QBO period in the chemically interactive models as compared with the chemically non-interactive models. However, it is difficult to fathom how the intensity of the secondary meridional circulation

associated with the QBO could change the QBO period due to the fact that any speedup or slowdown of the descending westerly shear zones is roughly compensated by the concurrent slowdown or speedup of the descending easterly shear zones. Furthermore, due to the increase of the zonal mean temperatures and ozone concentrations with the altitude in the lower stratosphere, the motion, ozone, and thermal waves are closely coupled. Pawson et al. (1992) found that the net linearized cooling coefficient from CO_2 (Newtonian cooling) was more than compensated in the lower equatorial atmosphere arising from absorption by the 9.6 μm bands of ozone (see their figure 8). This reduced or negative radiative damping in the lower stratosphere acts to lengthen the QBO period in presence of the increased ozone due to the doubling of the CO_2 concentrations. Finally, taking into account the short-wave heating of eddy ozone, Cordero et al. (1998) used a mechanistic model with a one-dimensional representation for mean flow and a three-dimensional depiction for Kelvin and Rossby-gravity waves to demonstrate that the ozone distribution, which maximizes in the middle stratosphere, leads to the local radiative damping decreases by up to 15% below 35 km and its increases by up to 20%. They concluded that ozone feedbacks lengthen the QBO period by about 2 months. Cordero and Nathan (2000) further developed a more sophisticated mechanistic model with a two-dimensional representation for mean flow and a three-dimensional depiction for Kelvin and Rossby-gravity waves, and surprisingly found that ozone feedbacks had little influence on the QBO period. We believe that more studies should be conducted to fully understand how to put together those various effects of interactive ozone on the QBO period.

Using the NASA Goddard Institute for Space Studies (GISS) Model E2.2-AP (Rind et al. 2020; Orbe et al. 2020), DallaSanta et al. (2021), to the great extent, isolated the overall effect on the QBO period of the increase in ozone due to the doubled CO_2. They first used a chemically non-interactive (NINT) model to conduct two CMIP6 experiments: the preindustrial (pi) control run, and the doubled CO_2 (2X) run. The two experiments only differ in the CO_2 concentration with the latter being two times the former.

Any other specification of these two experiments is the same, e.g., the ozone concentrations in the two runs are identical. Their Figure 5 shows that the doubling of CO_2 in the NINT model shortens the QBO period from 29.1 to 25 months. In other words, the doubling of CO_2 shortens the QBO period by 14%. DallaSanta et al. (2021) then employed a chemically interactive CMIP6 model with a mass-based scheme (Bauer et al., 2020), called One-Moment Aerosol (OMA), to conduct the pi control run and the 2X run. The ozone concentrations simulated by the OMA model increase by 10-15% in response to the doubling of CO_2 (figure not shown), which is consistent with the results of Jonsson et al. (2004). Figure 5 in DallaSanta et al. (2021) indicates that the doubling of CO_2 in the OMA model shortens the QBO period from 31.7 to 26.6 months. Namely, the doubling of CO_2 shortens the QBO period by 16%. In short, the results of DallaSanta et al. (2021) appear to suggest that three-way interactions among dynamics, chemistry, and radiation tend to slightly amplify the shortening of the QBO period in response to the doubling of CO_2.

Note that N, the Brunt-Väisälä frequency, in Eqs. (2) and (3) also changes with increasing CO_2. Richter et al. (2020b) showed that N^2 would be decreased by $\sim 5\%$ in the stratosphere when CO_2 is doubled (refer to their Figure 2c). We used the HL model to conduct a sensitivity test by adopting $G = 0$ in Eq. (1) with the radiative damping profile corresponding to the doubled CO_2 and the top of the models at the 48 km level. The rest of parameters in this sensitivity test are identical to those in all the previous runs except that the Brunt-Väisälä frequency in this experimental run was 2.5% smaller than that in the control run. The models were run for 1000 years to further increase the spectral resolution. We found that when the Brunt-Väisälä frequency was decreased by 2.5%, the simulated QBO period was slightly lengthened from 30 months to 30.2 months (figure not shown). In other words, the impact of decreasing stratospheric buoyancy frequency on the QBO period is almost negligible.

Analyzing eleven CCMI-1 REF-C2 climate–chemistry simulations, Eichinger and Šácha (2020) showed that the scale height in the stratosphere decreases by 2.3% per century. Accordingly, we used the HL model to conduct another sensitivity test by adopting $G = 0$ in Eq. (1) with the radiative damping profile corresponding to the doubled CO_2 and the top of the models at the 48 km level. The rest of parameters in this sensitivity test are identical to those in all the previous control runs except that the scale height in this experimental run was 2.3% smaller than that in the control run. The model was also run for 1000 years for the sake of higher spectral resolution. We found that when the scale height was decreased by 2.3%, the simulated QBO period was also shortened by about 2.3%, i.e., from 30 months to 29.3 months (figure not shown). Apparently, the shortening of the QBO period due to the warming climate is ascribed less to the shrinkage of the scale height in the stratosphere than to the enhancing of the stratospheric radiative damping. Together, the shrinking scale height and the increasing radiative damping shorten the QBO period by about 9.6%.

5. Conclusions

Plumb (1977) envisioned that stratospheric climate change would give rise to long-term changes in the QBO period due to changes in radiative damping and the Brunt-Väisälä frequency. Using one-dimensional (1D) models and taking into account the uncertainty due to the radiative damping rate, we found that the enhanced radiative damping arising from the doubling of CO_2 leads to the shortening of the QBO period by about $7.4\% \pm 0.9\%$ provided that the model top is higher than the 46 km level. Furthermore, when we incorporated both the 2.3% shrinkage of the scale height and the enhanced radiative damping, the QBO period is shortened by about 9.6%. In addition, the impact of decreasing stratospheric buoyancy frequency is marginal. While the increased ozone in response to the doubling of CO_2 appears to slightly further shorten the QBO period, more research needs to be done for the

appreciation of the underlying mechanisms. Note that those models include neither gravity waves nor tropical upwelling and assume that there are no changes in wave fluxes entering the equatorial stratosphere.

From a comprehensive model perspective, Richter et al. (2020b) showed that the changes in period of the QBO in warming climate simulations varied quite significantly among these models. Some models projected longer mean periods and some shorter mean periods for the QBO in a future warmer climate. They argue that uncertainty in the representation of the parameterized gravity waves is the most likely cause of the spread among the QBOi models in the QBO's response to climate change.

In addition, CO2 increases in the NASA GISS Model E2.2-AP lead to a decrease of both QBO period and QBO amplitude (DallaSanta et al., 2021). The period decrease is mostly associated with increases in lower stratospheric momentum fluxes (related to parameterized convection), a finding consistent with Geller et al. (2016a, 2016b) and Richter et al. (2020b). The amplitude decrease is mainly associated with a strengthened residual mean circulation, also consistent with the literature, although the vertical structure of the circulation response is nontrivial. It is worth mentioning that horizontal momentum flux divergences could also play an important role in weakening the QBO (Match and Fueglistaler, 2019, 2020).

Our 1D models only explored how the QBO period responds to the enhancing radiative damping of planetary waves, the shrinking scale height in the stratosphere, and the decreasing stratospheric buoyancy frequency due to the increasing CO_2 concentration. In order to investigate how those factors affect gravity waves which play an even more important role in determining the QBO period than planetary waves, high-resolution models such as those used by Kawatani et al. (2011, 2019) are desirable to further our understanding. Ultimately, how the QBO period changes in response to the increasing CO_2 will be determined by the combined effects of the strengthening of tropical upwelling, the increasing of

445 wave fluxes entering the equatorial stratosphere, the enhancing of radiative damping, and the shrinking
446 of the scale height in the stratosphere, which warrants further research.
447
448 **Data availability**
449 Any data used in this paper can be made available from the corresponding author upon request.
450
451 **Author contributions**
452 All authors made equal contributions to this work.
453
454 **Competing interests**
455 The authors declare that they have no conflict of interest.
456
457 **Acknowledgements:** Climate modeling at GISS is supported by the NASA Modeling, Analysis and
458 Prediction program, and resources supporting this work were provided by the NASA High-End
459 Computing (HEC) Program through the NASA Center for Climate Simulation (NCCS) at Goddard Space
460 Flight Center. KD acknowledges support from the NASA Postdoctoral Program. The authors thank the
461 editor Peter Haynes and two anonymous reviewers for their helpful comments, which led to an improved
462 paper. The authors also acknowledge very useful discussions with Drs. Geller and Orbe.
463
464 **References**
465 Andrews, D. G., Holton, J. R., and Leovy, C. B.: Middle Atmosphere Dynamics, Academic Press, 489
466 pp, 1987.

Baldwin, M. P., Gray, L. J., Dunkerton, T. J., Hamilton, K., Haynes, P. H., Randel, W. J., Holton, J. R., Alexander, M. J., Hirota, I., Horinouchi, T., Jones, D. B. A., Kinnersley, J. S., Marquardt, C., Sato, K., and Takahashi, M.: The Quasi-biennial oscillation, Rev. Geophys., 39, 179–229, https://doi.org/10.1029/1999RG000073, 2001.

Bauer, S. E., Tsigaridis, K., Faluvegi, G., Kelley, M., Lo, K. K., Miller, R. L., Nazarenko, L., Schmidt, G. A., and Wu, J.: Historical (1850–2014) Aerosol Evolution and Role on Climate Forcing Using the GISS ModelE2.1 Contribution to CMIP6, J. Adv. Model. Earth Sy., 12, e2019MS001978, https://doi.org/10.1029/2019ms001978, 2020.

Berk, A., Anderson, G. P., Acharya, P. K., Shettle, E. P.: MODTRAN5 version 2 user's manual, Spectral Sciences, Inc., Burlington MA and Air force Geophysics Laboratory, Hanscom AFB, MA, 2008.

Bushell, A. C., Jackson, D. R., Butchart, N., Hardiman, S. C., Hinton, T. J., Osprey, S. M., and Gray, L. J.: Sensitivity of GCM tropical middle atmosphere variability and climate to ozone and parameterized gravity wave changes, J. Geophys. Res., 115, D15101, https://doi.org/10.1029/2009JD013340, 2010.

Butchart, N.: The Brewer-Dobson circulation, Rev. Geophys., 52, 157–184, https://doi.org/10.1002/2013RG000448, 2014.

Butchart, N., Scaife, A. A., Bourqui, M., Grandpré, J., Hare, S. H., Kettleborough, J., Langematz, U., Manzini, E., Sassi, F., Shibata, K., Shindell, D. and Sigmond, M.: Simulations of anthropogenic change in the strength of the Brewer–Dobson circulation, Climate Dynamics, 27, 727–741, https://doi.org/10.1007/s00382-006-0162-4, 2006.

Butchart, N., Anstey, J., Hamilton, K., Osprey, S., McLandress, C., Bushell, A. C., Kawatani, Y., Kim, Y.-H., Lott, F., Scinocca, J., Stockdale, T.N., Andrews, M., Bellprat, O., Braesicke, P., Cagnazzo, C., Chen, C.-C., Chun, H.-Y., Dobrynin, M., Garcia, R., Garcia-Serrano, J., Gray, L.J., Holt, L.,

Kerzenmacher, T., Naoe, H., Pohlmann, H., Richter, J. H., Scaife, A.A., Schenzinger, V., Serva, F., Versick, S., Watanabe, S., Yoshida, K. and Yukimoto, S.: Overview of experiment design and comparison of models participating in phase 1 of the SPARC Quasi-Biennial Oscillation initiative (QBOi), Geoscientific Model Development, 11, 1009–1032. https://doi.org/10.5194/gmd-11-1009-2018, 2018.

Butchart, N., Anstey, J. A., Kawatani, Y., Osprey, S. M., Richter, J. H., Wu, T.: QBO changes in CMIP6 climate projections, *Geophys. Res. Lett.,* 47, 1–10. https://doi.org/10.1029/2019GL086903, 2020.

Camargo, S. J. and Sobel, A. H.: Revisiting the influence of the quasi-biennial oscillation on tropical cyclone activity, J. Climate, 23, 5810–5825, https://doi.org/10.1175%2F2010JCLI3575.1, 2010.

Cionni, I., Eyring, V., Lamarque, J. F., Randel, W. J., Stevenson, D. S., Wu, F., Bodeker, G. E., Shepherd, T. G., Shindell, D. T., and Waugh, D. W.: Ozone database in support of CMIP5 simulations: results and corresponding radiative forcing, Atmos. Chem. Phys., 11, 11267–11292, https://doi.org/10.5194/acp-11-11267-2011, 2011.

Collimore, C. C., Martin, D. W., Hitchman, M. H., Huesmann, A., and Waliser, D. E.: On the relationship between the QBO and tropical deep convection, J. Climate, 16, 2552–2568, https://doi.org/10.1175/1520-0442(2003)016%3C2552:OTRBTQ%3E2.0.CO;2, 2003.

Cordero, E. C., and Nathan, T. R.: The influence of wave- and zonal-mean ozone feedbacks on the quasi-biennial oscillation, J. Atmos. Sci., 57, 3426–3442, https://doi.org/10.1175/1520-0469(2000)057%3c3426:TIOWAZ%3e2.0.CO;2, 2000.

Cordero, E. C., Nathan, T. R., and Echols, R. S.: An analytical study of ozone feedbacks on Kelvin and Rossby–gravity waves: Effects on the QBO, J. Atmos. Sci., 55, 1051–1062, https://doi.org/10.1175/1520-0469(1998)055%3C1051:AASOOF%3E2.0.CO;2, 1998.

DallaSanta, K., Orbe, C., Rind, D., Nazarenko, L., and Jonas, J.: Dynamical and trace gas responses of the Quasi-Biennial Oscillation to increased CO_2, J. Geophys. Res. Atmos., 126, e2020JD034151. https://doi.org/10.1029/2020JD034151, 2021.

Dickinson, R. E.: Method of parameterization for infrared cooling between altitudes of 30 and 70 kilometers, J. Geophys. Res., 78, 4451–4457, https://doi.org/10.1029/JC078i021p04451, 1973.

Dunkerton, T. J.: The role of gravity waves in the quasi-biennial oscillation, J. Geophys. Res., 102, 26053–26076, https://doi.org/10.1029/96JD02999, 1997.

Ebdon, R. A.: Notes on the wind flow at 50 mb in tropical and subtropical regions in January 1957 and in 1958, Q. J. Roy. Meteor. Soc., 86, 540–542, https://doi.org/10.1002/qj.49708637011, 1960.

Eichinger, R. and Šácha, P.: Overestimated acceleration of the advective Brewer-Dobson circulation due to stratospheric cooling, Q. J. R. Meteorol. Soc., 1-15, https://doi.org/10.1002/qj.3876, 2020.

Fels, S. B.: A parameterization of scale-dependent radiative damping rates in the middle atmosphere, J. Atmos. Sci., 39, 1141–1152, https://doi.org/10.1175/1520-0469(1982)039%3C1141:APOSDR%3E2.0.CO;2, 1982.

Fels, S. B.: Radiative-dynamical interactions in the middle atmosphere, Advances in Geophysics, Vol. 28A, Academic Press, 277–300, https://doi.org/10.1016/S0065-2687(08)60227-7, 1985.

Garfinkel, C. I. and Hartmann, D. L.: The influence of the quasi-biennial oscillation on the troposphere in winter in a hierarchy of models. Part I: Simplified dry GCMs, J. Atmos. Sci., 68, 1273–1289, https://doi.org/10.1175%2F2011JAS3665.1, 2011a.

Garfinkel, C. I. and Hartmann, D. L.: The influence of the quasi-biennial oscillation on the troposphere in winter in a hierarchy of models. Part II: Perpetual winter WACCM runs, J. Atmos. Sci., 68, 2026–2041, https://doi.org/10.1175%2F2011JAS3702.1, 2011b.

534 Geller, M. A., Zhou, T., Shindell, D., Ruedy, R., Aleinov, I., Nazarenko, L., Tausnev, N. L., Kelley, M.,
535 Sun, S., Cheng, Y., Field, R. D., and Faluvegi, G.: Modeling the QBO-improvements resulting from
536 higher-model vertical resolution, J. Adv. Model. Earth Syst., 8, 1092–1105,
537 https://doi.org/10.1002/2016MS000699, 2016a.
538 Geller, M. A., Zhou, T., and Yuan, W.: The QBO, gravity waves forced by tropical convection, and
539 ENSO, J. Geophys. Res. Atmos., 121, 8886-8895, https://doi.org/10.1002/2015JD024125, 2016b.
540 Gidden, M. J., Riahi, K., Smith, S. J., Fujimori, S., Luderer, G., Kriegler, E., van Vuuren, D. P., van den
541 Berg, M., Feng, L., Klein, D., Calvin, K., Doelman, J. C., Frank, S., Fricko, O., Harmsen, M.,
542 Hasegawa, T., Havlik, P., Hilaire, J., Hoesly, R., Horing, J., Popp, A., Stehfest, E., and Takahashi,
543 K.: Global emissions pathways under different socioeconomic scenarios for use in CMIP6: a dataset
544 of harmonized emissions trajectories through the end of the century, Geosci. Model Dev., 12, 1443–
545 1475, https://doi.org/10.5194/gmd-12-1443-2019, 2019.
546 Giorgetta, M. A. and Doege, M. C.: Sensitivity of the Quasi-Biennial Oscillation to CO_2 doubling,
547 Geophys. Res. Lett., 32, L08701. https://doi.org/10.1029/2004GL021971, 2005.
548 Giorgetta, M. A., Bengtson, L., and Arpe, K.: An investigation of QBO signals in the east Asian and
549 Indian monsoon in GCM experiments, Climate Dynamics, 15, 435–450,
550 https://doi.org/10.1007/s003820050292, 1999.
551 Giorgetta, M. A., Manzini, E., and Roeckner, E.: Forcing of the quasi-biennial oscillation from a broad
552 spectrum of atmospheric waves, *Geophys. Res. Lett.*, 29, https://doi.org/10.1029/2002GL014756,
553 2002.
554 Giorgetta, M. A., Manzini, E., and Roeckner, E., Esch, M., and Bengtsson, L.: Climatology and forcing
555 of the quasi-biennial oscillation in the MAECHEM5 model, J. Climate, 19, 3882–3901,
556 https://doi.org/10.1175/JCLI3830.1, 2006.

557 Gray, W. M.: Atlantic seasonal hurricane frequency. Part I: El Niño and 30-mb quasi-biennial oscillation
558 influences, Mon. Wea. Rev., 112, 1649–1688, https://doi.org/10.1175/1520-
559 0493(1984)112%3C1649:ASHFPI%3E2.0.CO;2, 1984.
560 Gray, W. M., Sheaffer, J. D., and Knaff, J.: Influence of the stratospheric QBO on ENSO variability, J.
561 Meteor. Soc. Jpn., 70, 975–995, https://doi.org/10.2151/jmsj1965.70.5_975, 1992.
562 Hamilton, K.: The vertical structure of the quasi-biennial oscillation: Observations and theory, Atmos.
563 Ocean, 19, 236–250, http://dx.doi.org/10.1080/07055900.1981.9649111, 1981.
564 Hansen, F., Matthes, K., and Wahl, S.: Tropospheric QBO–ENSO interactions and differences between
565 the Atlantic and Pacific, J. Climate, 29, 1353–1368, https://doi.org/10.1175/JCLI-D-15-0164.1,
566 2016
567 Hasebe, F.: Quasi-biennial oscillations of ozone and diabatic circulation in the equatorial stratosphere, J.
568 Atmos. Sci., 51, 729–745, https://doi.org/10.1175/1520-
569 0469(1994)051%3c0729:QBOOOA%3e2.0.CO;2, 1994.
570 Hitchman, M. H., and Huesmann, A. S.: Seasonal influence of the quasi-biennial oscillation on
571 stratospheric jets and Rossby wave breaking, J. Atmos. Sci., 66, 935–946,
572 https://doi.org/10.1175%2F2008JAS2631.1, 2009.
573 Ho, C.-H., Kim, H.-S., Jeong, J.-H., and Son, S.-W.: Influence of stratospheric quasi-biennial oscillation
574 on tropical cyclone tracks in the western North Pacific, Geophys. Res. Lett., 36, L06702,
575 http://dx.doi.org/10.1029/2009GL037163, 2009.
576 Holt, L., Lott, F., Garcia, R., Kiladis, G.N., Anstey, J.A., Braesicke, P., Bushell, A.C., Butchart, N.,
577 Cagnazzo, C., Chen, C.-C., Chun, H.-Y., Hamilton, K., Kawatani, Y., Kerzenmacher, T., Kim, Y.-
578 H., McLandress, C., Naoe, H., Osprey, S., Richter, J.H., Scinocca, J., Serva, F., Versick, S.,

579 Watanabe, S., Yoshida, K., and Yukimoto, S.: An evaluation of tropical waves and wave forcing of
580 the QBO in the QBOi models, Q. J. R. Meteorol. Soc., https://doi.org/10.1002/qj.3827, 2020.
581 Holton, J. R. and Lindzen, R. S.: An updated theory for the quasi-biennial cycle of the tropical
582 stratosphere, J. Atmos. Sci., 29, 1076–1080, https://doi.org/10.1175/1520-
583 0469(1972)029%3c1076:AUTFTQ%3e2.0.CO;2, 1972.
584 Holton, J. R. and Tan, H.: The Influence of the equatorial quasi-biennial oscillation on the global
585 circulation at 50 mb, J. Atmos. Sci., 37, 2200–2208, https://doi.org/10.1175/1520-
586 0469(1980)037%3c2200:TIOTEQ%3e2.0.CO;2, 1980.
587 Huang, B. H., Hu, Z. Z., Kinter, J. L., Wu, Z. H., and Kumar, A.: Connection of stratospheric QBO with
588 global atmospheric general circulation and tropical SST. Part I: Methodology and composite life
589 cycle, Climate Dynamics, 38, 1–23, https://doi.org/10.1007%2Fs00382-011-1250-7, 2012.
590 Jin, Z., Zhang, Y.-C., Del Genio, A., Schmidt, G., and Kelley, M.: Cloud scattering impact on thermal
591 radiative transfer and global longwave radiation, J. Quant. Spectrosc. Radiat. Transfer, 239, 106669,
592 https://doi.org/10.1016/j.jqsrt.2019.106669, 2019.
593 Jonsson, A., de Grandpre, J., Fomichev, V., McConnell, J., and Beagley, S.: Doubled CO2-induced
594 cooling in the middle atmosphere: Photochemical analysis of the ozone radiative feedback, J.
595 Geophys. Res., 109, D24103, https://doi.org/10.1029/2004JD005093, 2004.
596 Kawatani, Y. and Hamilton, K.: Weakened stratospheric Quasi-Biennial Oscillation driven by increased
597 tropical mean upwelling, Nature, 497, 478–481, https://doi.org/10.1038/nature12140, 2013.
598 Kawatani, Y., Takahashi, M., Sato, K., Alexander, S. P., and Tsuda, T.: Global distribution of
599 atmospheric waves in the equatorial upper troposphere and lower stratosphere: AGCM simulation
600 of sources and propagation, J. Geophys. Res., 114, D01102, https://doi.org/10.1029/2008JD010374,
601 2009.

Kawatani, Y., Watanabe, S., Sato, K., Dunkerton, T. J., Miyahara, S., and Takahashi, M.: The roles of equatorial trapped waves and internal inertia-gravity waves in driving the Quasi-Biennial oscillation. Part I: Zonal mean wave forcing, J. Atmos. Sci., 67, 963–980, https://doi.org/10.1175/2009JAS3222.1, 2010.

Kawatani, Y., Hamilton, K., and Watanabe, S.: The quasi-biennial oscillation in a double CO2 climate, J. Atmos. Sci., 68, 265–283, https://doi.org/10.1175/2010JAS3623.1, 2011.

Kawatani, Y, Lee, J. N., and Hamilton, K.: Interannual variations of stratospheric water vapor in MLS observations and climate model simulations, J. Atmos. Sci., 71, 4072–4085, https://doi.org/10.1175/JAS-D-14-0164.1, 2014.

Kawatani, Y., Hamilton, K., Sato, K., Dunkerton, T. J., Watanabe, S., and Kikuchi, K.: ENSO Modulation of the QBO: Results from MIROC Models with and without Nonorographic Gravity Wave Parameterization, J. Atmos. Sci., 76, 3893–3917, https://doi.org/10.1175/JAS-D-19-0163.1, 2019.

Keeble, J., Hassler, B., Banerjee, A., Checa-Garcia, R., Chiodo, G., Davis, S., Eyring, V., Griffiths, P. T., Morgenstern, O., Nowack, P., Zeng, G., Zhang, J., Bodeker, G., Cugnet, D., Danabasoglu, G., Deushi, M., Horowitz, L. W., Li, L., Michou, M., Mills, M. J., Nabat, P., Park, S., and Wu, T.: Evaluating stratospheric ozone and water vapor changes in CMIP6 models from 1850–2100, Atmos. Chem. Phys. Discuss. [preprint], https://doi.org/10.5194/acp-2019-1202, in review, 2020.

Labitzke, K.: On the interannual variability of the middle stratosphere during the northern winters, J. Meteorol. Soc. Jpn., 80, 963–971, http://doi.org/10.2151/jmsj1965.60.1_124, 1982.

Lait, L. R., Schoeberl, M. R., and Newman, P. A.: Quasi-biennial modulation of the Antarctic ozone depletion, J. Geophys. Res., 94, 11559–11571, http://dx.doi.org/10.1029/JD094iD09p11559, 1989.

623 Li, F., Austin, J., and Wilson, R. J.: The strength of the Brewer–Dobson circulation in a changing climate:
624 Coupled chemistry–climate model simulations, J. Climate, 21, 40–57,
625 https://doi.org/10.1175/2007JCLI1663.1, 2008.
626 Liess, S. and Geller, M. A.: On the relationship between QBO and distribution of tropical deep
627 convection, J. Geophys. Res., 117, D03108, http://dx.doi.org/10.1029/2011JD016317, 2012.
628 Lindzen, R. S.: Equatorial planetary waves in shear: Part I, J. Atmos. Sci. 28, 609-622,
629 https://doi.org/10.1175/1520-0469(1971)028%3C0609:EPWISP%3E2.0.CO;2, 1971.
630 Lindzen, R. S. and Holton, J. R.: A theory of the quasi-biennial oscillation, J. Atmos. Sci., 25, 1095–
631 1107, https://doi.org/10.1175/1520-0469(1968)025%3C1095:ATOTQB%3E2.0.CO;2, 1968.
632 Marshall, A. G. and Scaife, A. A.: Impact of the QBO on surface winter climate, J. Geophys. Res., 114,
633 D18110, http://dx.doi.org/10.1029/2009JD011737, 2009.
634 Match, A., and Fueglistaler, S.: The buffer zone of the quasi-biennial oscillation, J. Atmos. Sci., 76, 3553–
635 3567, https://doi.org/10.1175/JAS-D-19-0151.1, 2019
636 Match, A., and Fueglistaler, S.: Mean-flow damping forms the buffer zone of the quasi-biennial
637 oscillation: 1D theory. J. Atmos. Sci., 77, 1955–1967, https://doi.org/10.1175/JAS-D-19-0293.1,
638 2020.
639 Matsuno, T.: Numerical integrations of primitive equations by use of a simulated backward difference
640 method, J. Meteor. Soc. Japan, 44, 76–84, https://doi.org/10.2151/jmsj1965.44.1_76, 1966.
641 Orbe, C., Rind, D., Jonas, J., Nazarenko, L., Faluvegi, G., Murray, L.T., Shindell, D.T., Tsigaridis, K.,
642 Zhou, T., Kelley, M., and Schmidt, G.: GISS Model E2.2: A climate model optimized for the middle
643 atmosphere. Part 2: Validation of large-scale transport and evaluation of climate response, *J.*
644 *Geophys. Res. Atmos.*, 125, e2020JD033151, https://doi.org/10.1029/2020JD033151, 2020.

Pawson, S., Harwood, R. S., and Haigh, J. D.: A study of the radiative dissipation of planetary waves using satellite data, *J. Atmos. Sci.*, 49, 1304–1317, https://doi.org/10.1175/1520-0469(1992)049%3C1304:ASOTRD%3E2.0.CO;2, 1992.

Plumb, R. A.: The interaction of two internal waves with the mean flow: Implications for the theory of the quasi-biennial oscillation, J. Atmos. Sci., 34, 1847–1858, https://doi.org/10.1175/1520-0469(1977)034<1847:TIOTIW>2.0.CO;2, 1977.

Reed, R. J., Campbell, W. J., Rasmussen, L. A., and Rogers, D. G.: Evidence of a downward-propagating, annual wind reversal in the equatorial stratosphere, J. Geophys. Res., 66, 813–818, http://dx.doi.org/10.1029/JZ066i003p00813, 1961.

Richter, J. H., Anstey, J. A., Butchart, N., Kawatani, Y., Meehl, G. A., Osprey, S., & Simpson, I. R., 2020b: Progress in simulating the quasi-biennial oscillation in CMIP models. Journal Geophysical Research: Atmospheres, 125, e2019JD032362, https://doi.org/10.1029/2019JD032362, 2020a.

Richter, J. H., Butchart, N., Kawatani, Y., Bushell, A. C., Holt, L., Serva, F., Anstey, J., Simpson, I. R., Osprey, S., Hamilton, K., Braesicke, P., Cagnazzo, C., Chen, C.-C., Garcia, R. R., Gray, L. J., Kerzenmacher, T., Lott, F., McLandress, C., Naoe, H., Scinocca, J., Stockdale, T. N, Versick, S., Watanabe, S., Yoshida, K., Yukimoto, S.: Response of the Quasi-Biennial Oscillation to a warming climate in global climate models, Q. J. R. Meteorol. Soc., 1–29. https://doi.org/10.1002/qj.3749, 2020b.

Rind, D., Jonas, J., Balachandran, N., Schmidt, G., and Lean, J.: The QBO in two GISS global climate models: 1. Generation of the QBO, J. Geophys. Res. Atmos., 119, 8798–8824, https://doi.org/10.1002/2014JD021678, 2014.

Rind, D., Orbe, C., Jonas, J., Nazarenko, L., Zhou, T., Kelley, M., Lacis, A., Shindell, D., Faluvegi, Russell, G., Bauer, M., Schmidt, G., Romanou, A., and Tausnev, N.: GISS Model E2.2: A climate

model optimized for the middle atmosphere — Model structure, climatology, variability and climate sensitivity, J. Geophys. Res. Atmos., 125, e2019JD032204, https://doi.org/10.1029/2019JD032204, 2020.

Saravanan, R.: A multiwave model of the quasi-biennial oscillation, J. Atmos. Sci., 47, 2465–2474, https://doi.org/10.1175/1520-0469(1990)047%3C2465:AMMOTQ%3E2.0.CO;2, 1990.

Scaife, A. A., Butchart, N., Warner, C. D., Stainforth, D., Norton, W., and Austin, J.: Realistic quasi-biennial oscillations in a simulation of the global climate, Geophys. Res. Lett., 27, 3481–3484, https://doi.org/10.1029/2000GL011625, 2000.

Schirber, S., Manzini, E., Krismer, T. and Giorgetta, M.: The Quasi-Biennial Oscillation in a warmer climate: sensitivity to different gravity wave parameterizations, Climate Dynamics, 45, 825–836, https://doi.org/10.1007/s00382-014-2314-2, 2015.

Trepte, C. R. and Hitchman, M. H.: Tropical stratospheric circulation deduced from satellite aerosol data, Nature, 355, 626–628, https://doi.org/10.1038/355626a0, 1992.

Watanabe, S. and Kawatani, Y.: Sensitivity of the QBO to mean tropical upwelling under a changing climate simulated with an Earth System Model, Journal of the Meteorological Society of Japan, Series II, 90A, 351–360, https://doi.org/10.2151/jmsj.2012-A20, 2012.

Yoo, C. and Son, S.-W.: Modulation of the boreal wintertime Madden-Julian oscillation by the stratospheric quasi-biennial oscillation, Geophys. Res. Lett., 43, 1392–1398, https://doi.org/10.1002%2F2016GL067762, 2016.

Zawodny, J. M. and McCormick, M. P.: Stratospheric Aerosol and Gas Experiment II measurements of the quasi-biennial oscilla- tions in ozone and nitrogen dioxide, J. Geophys. Res., 96, 9371– 9377, http://dx.doi.org/10.1029/91JD00517, 1991.

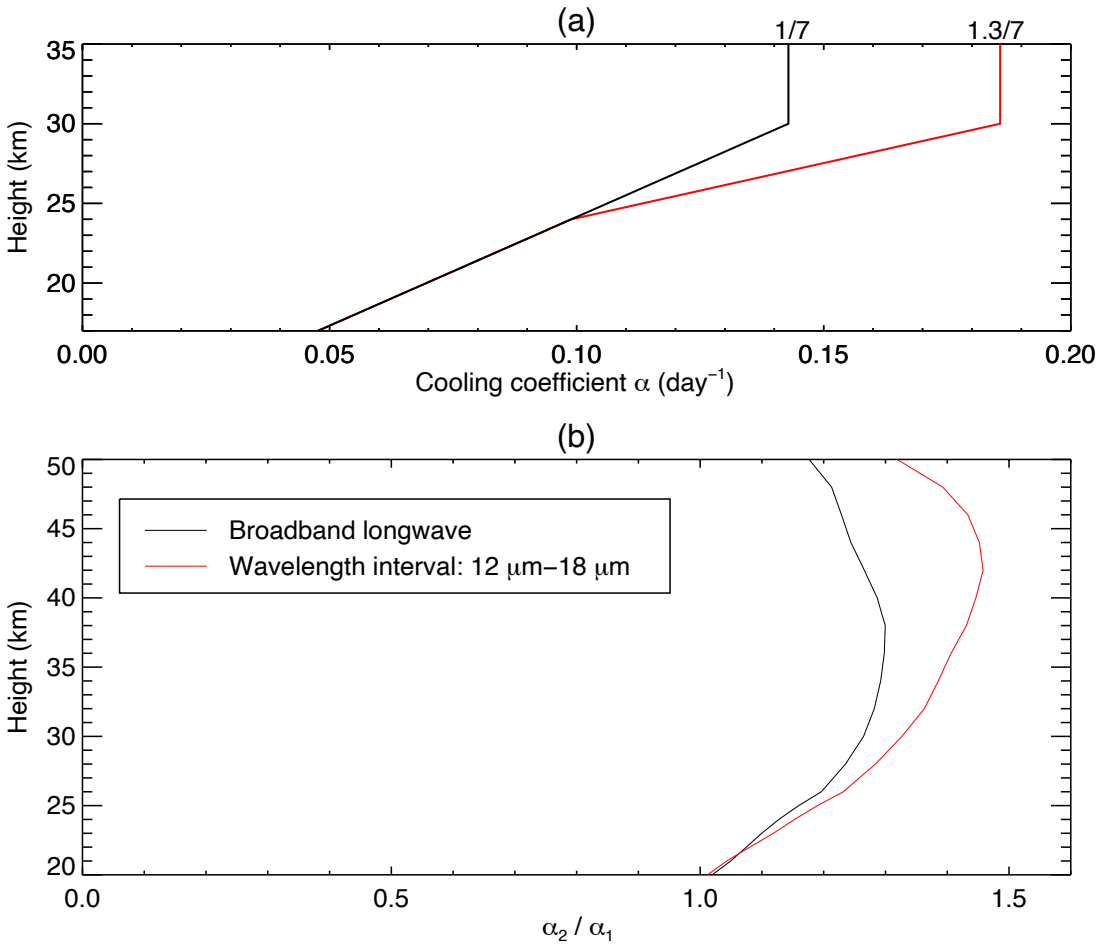

FIG. 1: (a) Profiles of Newtonian cooling coefficients: The smaller values (black line) are used for the control runs while the larger values (red line) are used for the experimental runs. (b) Profiles of the ratio of α_2 to α_1, where α_1 and α_2 denote the Newtonian cooling coefficient for the reference CO_2 and the doubled CO_2, respectively. The black line depicts the ratio for the broadband longwave ($5\ \mu m - 100\ \mu m$) and the red line delineates that for the CO_2 absorption band ($12\ \mu m - 18\ \mu m$).

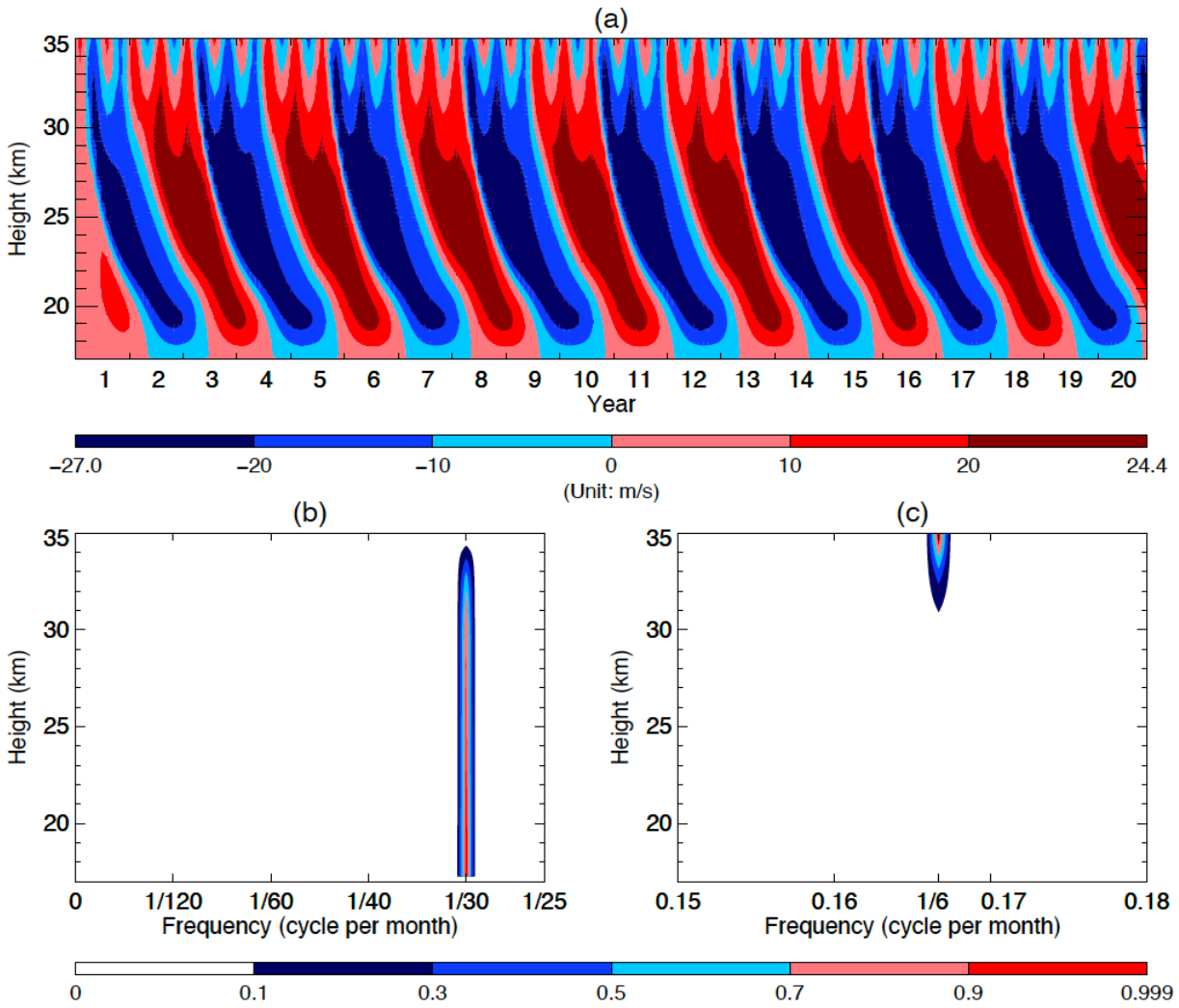

FIG. 2: (a) Time–height section of the monthly averaged mean zonal wind over the first 20 years from the HL's original model. (b) and (c) Frequency–height section of the power spectral densities (PSD) of the standardized monthly averaged mean zonal wind of the 100 years. Note that in order to better visualize the PSD in (b) and (c), we trimmed off the blank segments for the frequencies ranging from $\frac{1}{25}$ to 0.15 cycle per month and those ranging from 0.18 to 0.5 cycle per month.

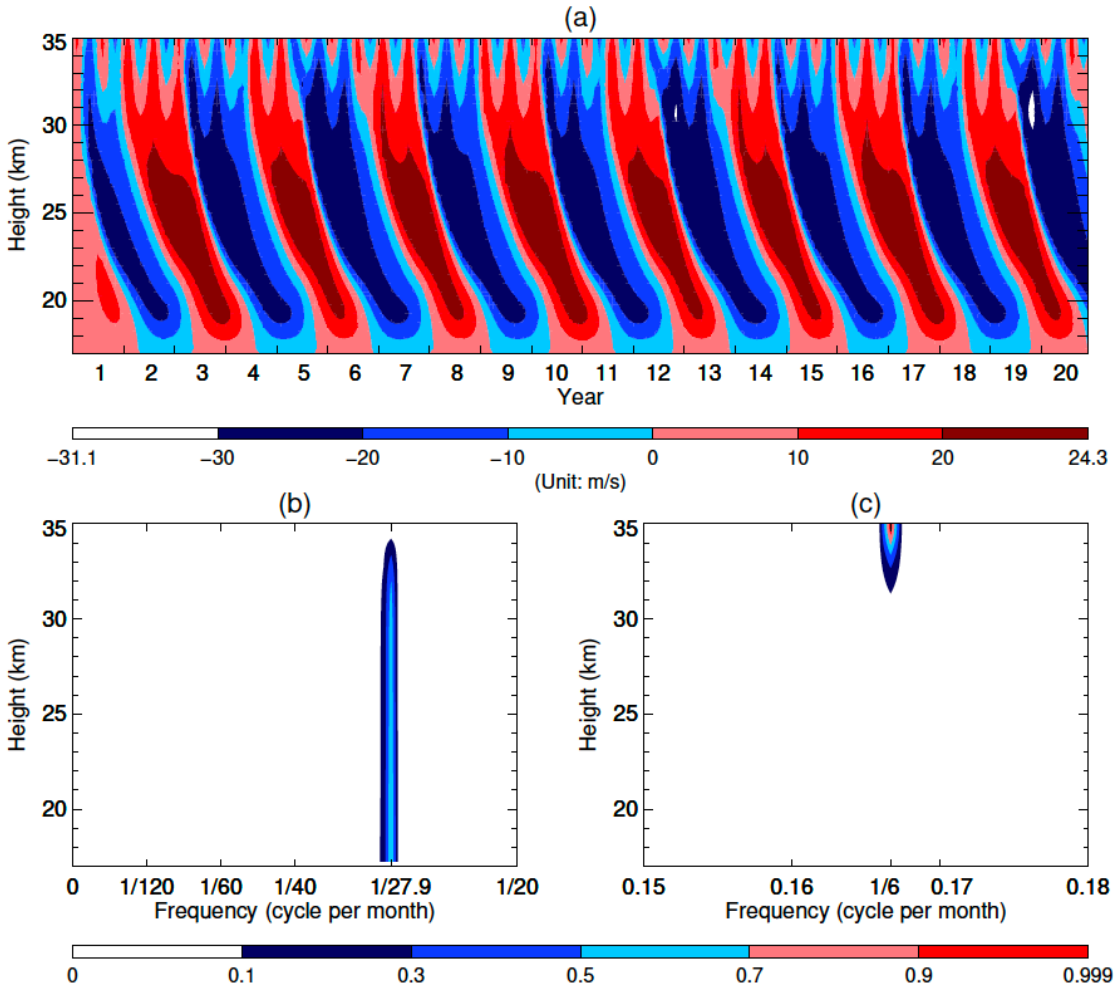

FIG. 3: (a) Same as FIG. 2a, but with the enhanced $\alpha(z)$ depicted as the red line in FIG. 1a. (b) and (c) Frequency–height section of the power spectral densities (PSD) of the standardized monthly averaged mean zonal wind of the 100 years. Note that in order to better visualize the PSD in (b) and (c), we trimmed off the blank segments for the frequencies ranging from $\frac{1}{20}$ to 0.15 cycle per month and those ranging from 0.18 to 0.5 cycle per month.

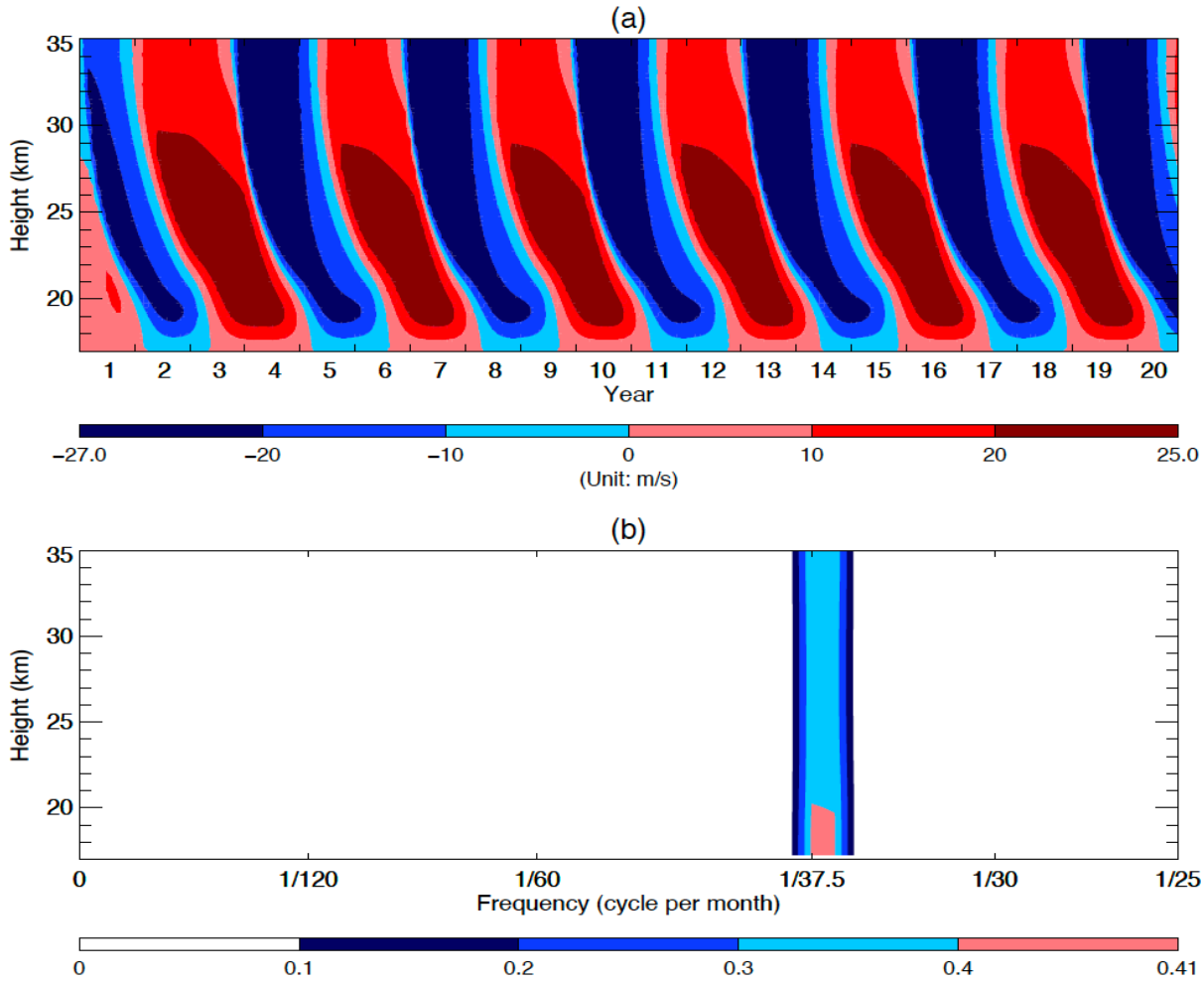

FIG. 4: (a) Time–height section of the monthly averaged mean zonal wind over the first 20 years from the HL's model without the semiannual forcing. (b) Frequency–height section of the power spectral densities (PSD) of the standardized monthly averaged mean zonal wind of the 100 years. Note that in order to visualize the PSD, we trimmed off the blank segment for the frequencies ranging from $\frac{1}{25}$ to 0.5 cycle per month.

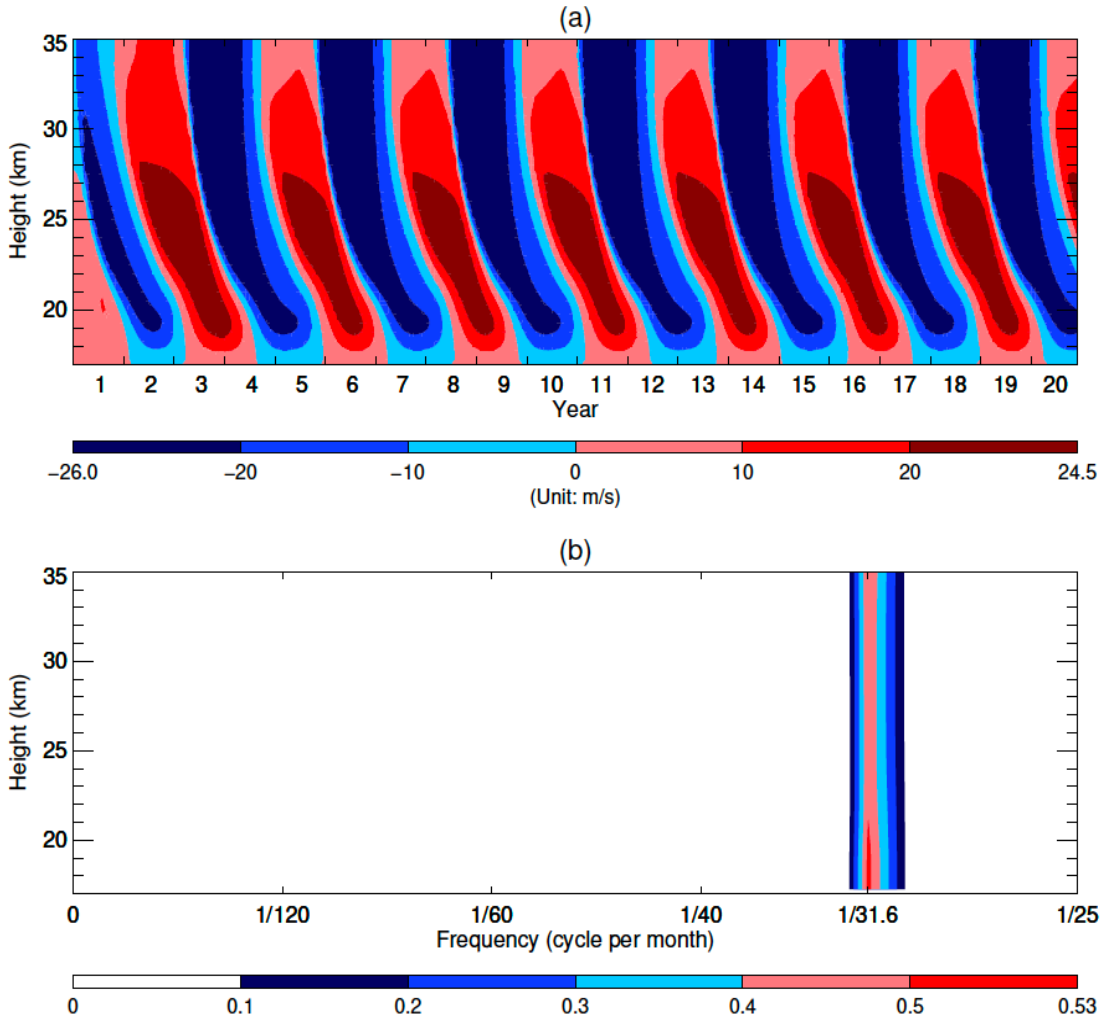

FIG. 5: (a) Same as FIG. 4a, but with the enhanced $\alpha(z)$ depicted as the red line in FIG. 1a. (b) Same as FIG. 4b, but for the doubled CO_2 Run.

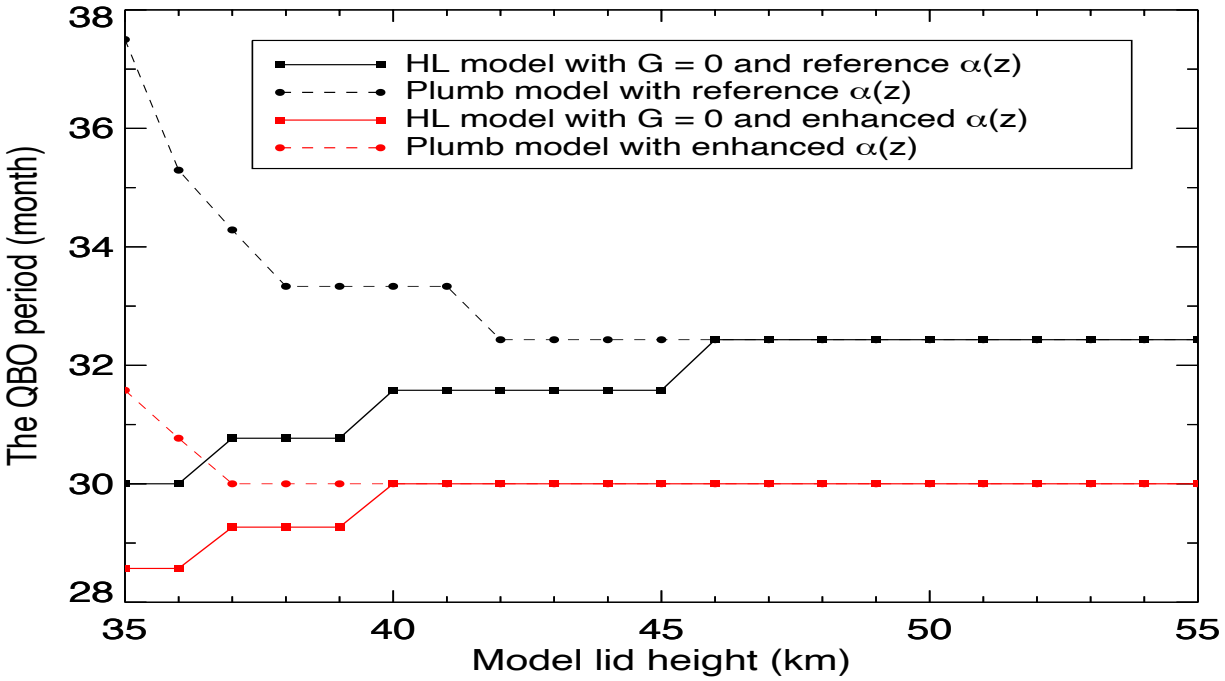

FIG. 6: The relationship between the simulated QBO period with the height of the model lid. Black and red lines depict the results from using the reference radiative damping and the enhanced radiative damping respectively while solid and dashed lines delineate the results from the HL model with $G = 0$ and the Plumb model respectively.